Continental Shelf Currents in Tropical Storm Delia: Observations and Theory

GEORGE Z. FORRISTALL

Shell Development Company, Houston, Tex. 77001

ROBERT C. HAMILTON

Evans-Hamilton, Inc., Houston, Tex. 77072

VINCENT J. CARDONE

Institute of Marine and Atmospheric Sciences, City University of New York, New York, N.Y. 10031

(Manuscript received 12 November 1976, in revised form 21 February 1977)

ABSTRACT

Storm currents are a significant part of the design hydrodynamic flow field in areas subject to tropical storms. In September 1973, Tropical Storm Delia passed over the instrumented Buccaneer platform located in 20 m of water 50 km south of Galveston, Tex. Current meter records from three depths show the storm produced currents on the order of 2 m s^{-1} which persisted to near the bottom. A mathematical model of wind-driven current generation was successful in hindcasting the observed current development after a linear slip condition bottom was incorporated in the model.

1. Introduction

The design of an offshore structure is dependent on the size of the storm waves which the structure is expected to endure during its life span. Increasingly sophisticated methods have been developed for calculating the wave climatology in a given region based on relatively short wave height records (Cardone *et al.*, 1976).

However, it is important to remember that for design we are not interested only in the wave heights *per se*, but also in the velocities and accelerations of the water particles as they impinge on the structure.

The oscillatory motions due to the waves can be theoretically calculated given a history of the sea surface height, but slowly varying velocities due to currents are usually present also and the wave climatology is of no help in predicting their magnitude. Forces due to the fluid motion are typically calculated using Morison's equation, which breaks the force into drag and inertial components. Since the drag in Morison's equation is proportional to the square of the velocity, adding a current with half the magnitude of the wave orbital velocity would more than double the calculated drag force.

Large currents can thus be important. Very little is known about currents during storms because of the obvious measurement difficulties. It was against this background that the Ocean Current Measurement Program was begun with a pilot measurement station in 1971 (Hall, 1972).

The measurement program now consists of three stations, whose locations in the northern Gulf of Mexico off the Texas and Louisiana coasts are shown in Fig. 1. The stations are on production platforms from 25 to 145 km offshore in water depths from 20 to 100 m. At each station, the instrumentation consists of an Aerovane, a wave staff, a barometer, and three or four current meters (Fig. 2).

Even with excellent data from several storms, it would be necessary to analyze the data within the framework of a theory of current generation to develop hindcast techniques and design parameters. Such theoretical work has progressed throughout the measurement program. A basic numerical model was developed (Forristall, 1974) which calculated time-dependent current profiles from assumed wind records. This model was preliminary in the sense that while based on fundamental hydrodynamic theory, it contained semi-empirical parameters which could only be properly evaluated through comparison of the model with current measurements during storms.

The overall success of the program thus depends ultimately on the vagaries of the weather. Two years of preparation and waiting were finally rewarded when Tropical Storm Delia passed almost directly over our Buccaneer station in September 1973. This paper describes the currents measured during the storm and the modifications made to the basic numerical model in order to successfully hindcast these currents.

2. Tropical Storm Delia

Satellite photographs in late August located an area of increasing cloudiness in the southwestern Carribean

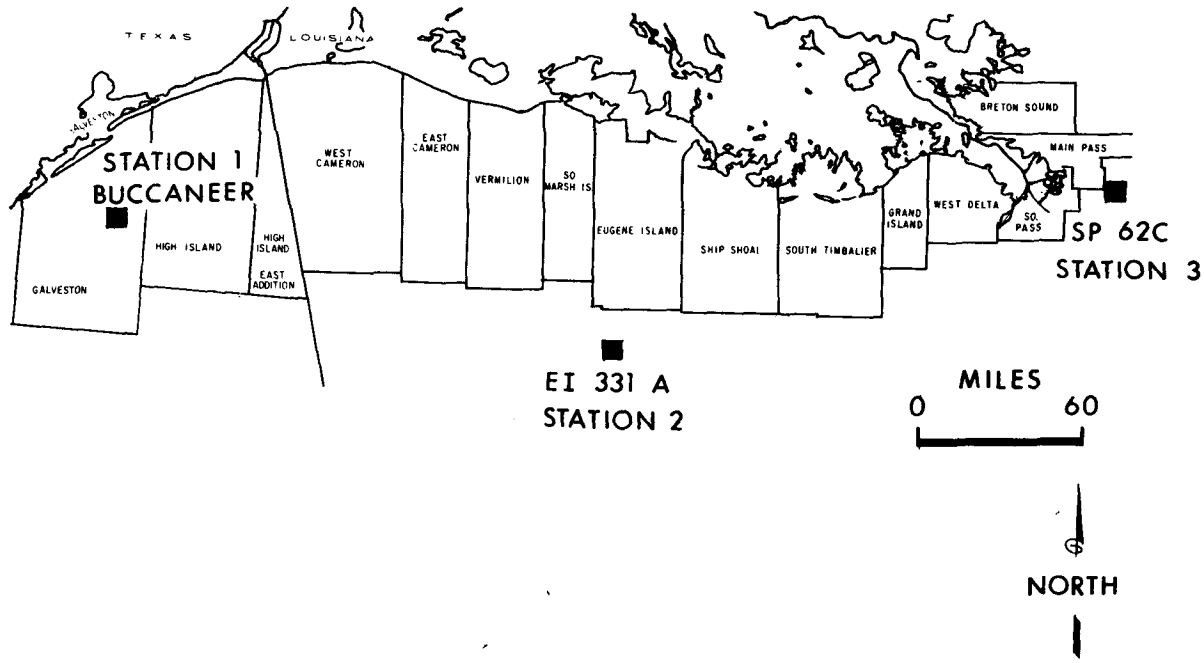

FIG. 1. Location map for measurement stations.

which later proved to be the formation of Tropical Storm Delia. This area of cloudiness and showers formed into a weak cyclonic circulation on 31 August and it continued to strengthen to become Tropical Storm Delia late on 2 September near 24°N, 88°W. Fig. 3 gives the storm track of Delia.

Delia deepened during the night of the 2nd and the morning of the 3rd, and took up a northwesterly course toward Galveston, Tex. Delia continued on a fairly regular northwesterly course during the morning of the 4th, and passed near the Buccaneer station during the afternoon of the 4th. Delia became erratic with an ill-defined center late on the 4th when it crossed the Texas coast near Galveston.

Although Delia was a relatively weak storm, it passed close enough to Buccaneer to produce a minimum pressure of 987 mb and a peak wind gust of 32 m s^{-1}. Analysis of the wind field indicates that these measurements were near the extreme values for the storm. The maximum wave heights were 7–8 m.

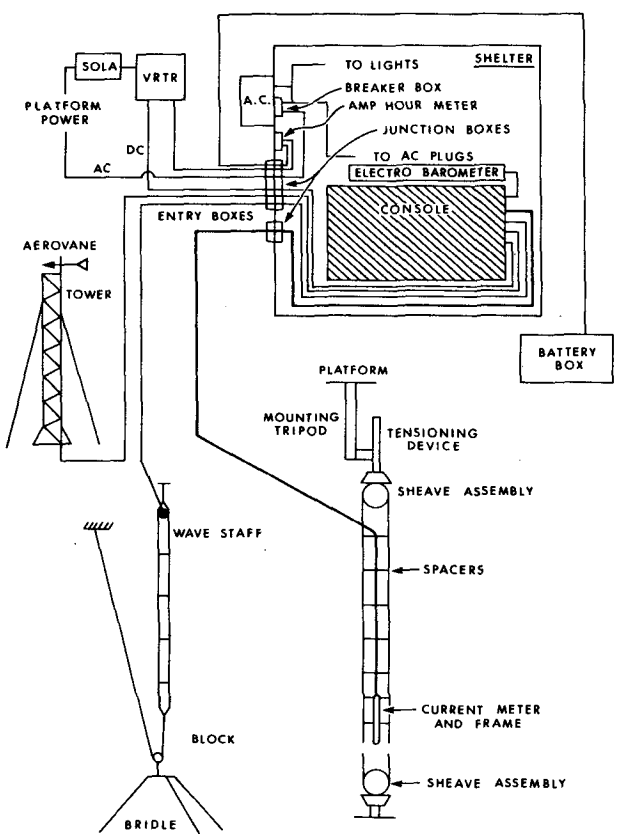

FIG. 2. Schematic diagram of instrumentation system.

3. Measurements

Fig. 4 shows a general view of the Buccaneer platform, located in 20 m of water. All of the primary transducers, with the exception of the electrobarometer, are installed near the center of the 200 ft bridge. The current meter array is visible in the photograph. The support system for the current meters is a pair of taut wires suspended between the bridge and an 18 000 lb steel anchor. The taut wires are constructed so that the three current meters are readily accessible and can be raised or lowered easily. The wave staff is located 6 ft from the current meter array; it is also suspended between the anchor and the bridge. The Aerovane is located near the bridge center on a 30 ft tower at a total elevation of ~98 ft above mean sea level. The structure closest to the suspended

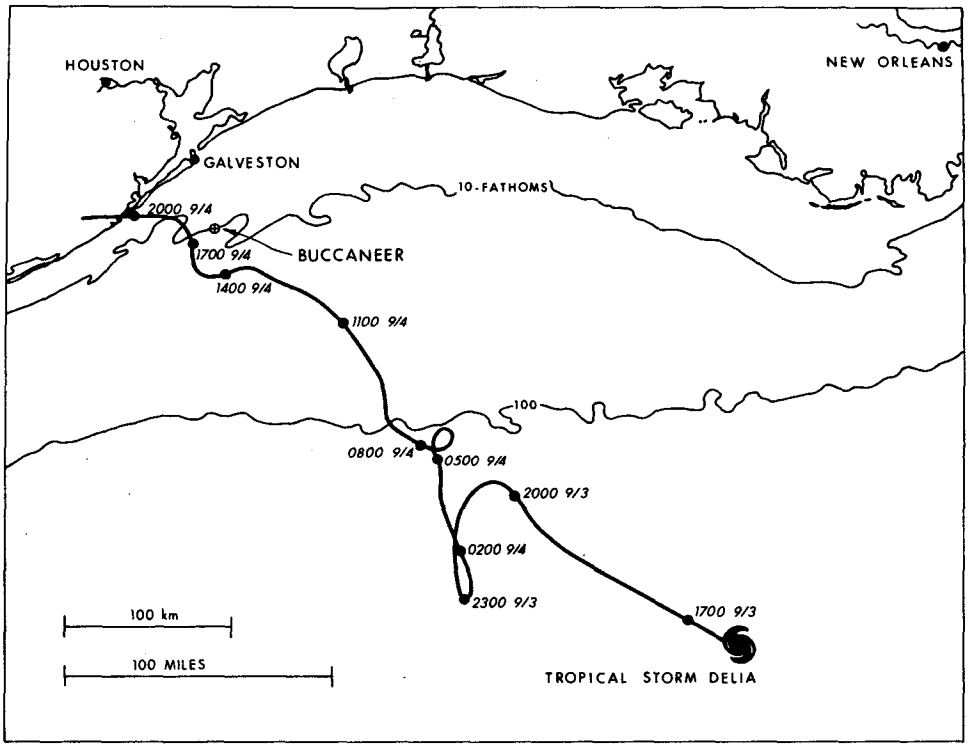

FIG. 3. Storm track of Tropical Storm Delia, September 1973. All times are CDT.

transducer array is the quarters platform, which is located 75 ft to the south of the anchor. The depths of the current meters are shown in Fig. 5.

The current meters used are based on Faraday's principle and have no moving parts. Thus, fouling and mechanical failure problems common to rotor-type instruments are of little concern. The meters have an extremely fast response time which is critical for accurate current measurements in the presence of large waves; it also makes possible a study of wave kinematics, which is in progress.

The Buccaneer station was visited on 30 August 1973 for routine maintenance and monthly tape changing. The station was found to be in excellent condition with the exception of an inoperative wave staff transducer. Since field repairs of this instrument are impossible and no spare was available, the wave staff was left off. When it became evident that Delia would affect the station, a spare transducer was procured and installed on 3 September, with the result that a complete data set of excellent quality was collected during the storm.

Although the instruments at Buccaneer performed well, we later discovered a mechanical problem which bears on the reliability of the current meter data. During December 1973, the current meters were raised for maintenance and the system was carefully inspected. We discovered that the taut wires were no longer parallel. This could only have been caused by a rotation of the anchor on the bottom, since the configuration on the work platform had not changed. It proved rather easy to accurately measure the amount of rotation by optical means and the calculated anchor rotation was 31°. Using a plumb to measure the inclination of the cables to the vertical and knowledge of the spot from which the anchor was originally lowered, it was also possible to calculate the absolute motion of the bottom sheave and block. These measurements were not as accurate as those for the rotation, but it appears that the sheave moved about 3 ft east and the block moved a few inches west. These measurements are compatible with a rotation of 31°.

Inspection of the anchor by a diver proved that the anchor had shifted position in a large scour hole. Since the current meters are geographically oriented by the taut wires, any rotation of the plane of taut wires causes a rotation of the measured current direction. Thus, after the indicated rotation, the direction north as indicated by the current meters was actually 018° true for meter 1, 023° true for meter 2 and 029° true for meter 3.

It has been impossible to determine when the rotation occurred, although it was most likely during the storm. If the rotation happened suddenly, the time of the movement could be found by inspection of the current meter records, but this was apparently not the case. Since the analysis of the current meter records was thus done without any rotation correction, it must be recognized that there is some uncertainty in the reported current directions.

4. Data analysis

The field data are recorded on two 7-track Geotech analog tape recorders at 0.03 inch per second (ips), which have essentially flat response up to 5 Hz. The tapes were then digitized at a playback speed of 7.5 ips with a sampling rate of 500 Hz and a 160 Hz anti-aliasing filter. The corresponding real time rates were 2 Hz digitization and 0.64 Hz low-pass filtering. The filter characteristics are shown in Fig. 6.

The field data tapes included automatic calibration records written on the tapes every 24 h. For most channels, the calibration mark is simply a constant voltage applied to the recorder. However, the current meters include an internal calibration circuit which also permits a check on the operation of most of the meter's amplification stages. Since the digital tapes also include the calibration marks, it is possible to calibrate the digital tapes to engineering units without a detailed knowledge of the performance of all the recorders and amplifiers upstream from the digital tapes. Confidence in the calibrated data is also increased by the fact that the calibration records were constant to well within 1% over the 8 days digitized.

The current meters used in the program do not have a perfect cosine response, i.e., for constant flow speed, the measured velocity is a nonconstant function of azimuth. The maximum error, for a current at 45° to the current meter axes, is 8%. According to the manufacturer, the response curve is fully repeatable for all meters of the design used in the program and for all flow velocities. Thus, the correct velocity $\mathbf{V}_c$ can be found from

$$\mathbf{V}_c=\mathbf{V}(1-0.08|\sin 2\theta|)^{-1}, \qquad (1)$$

which was applied to all the digitized and calibrated current meter records.

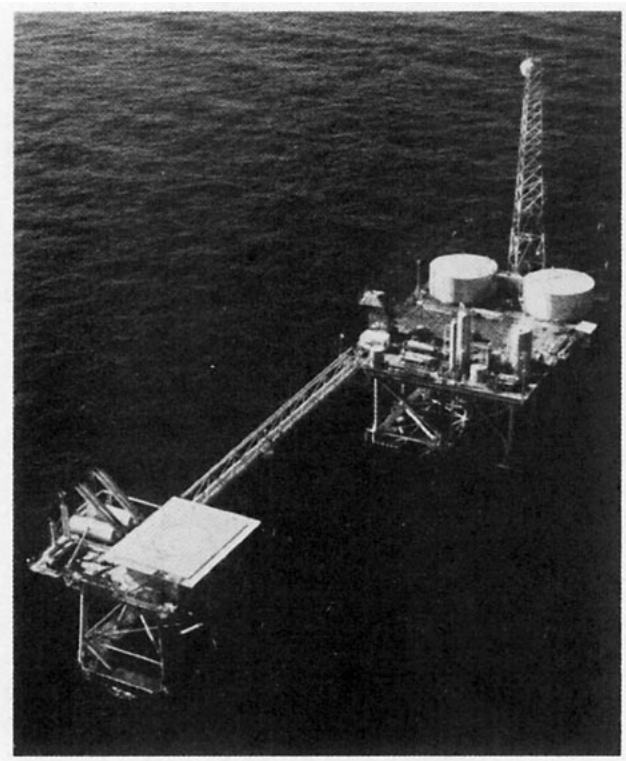

FIG. 4. Buccaneer A platform. Current meter taut wires, wave staff and anemometer tower are near the center of the bridge.

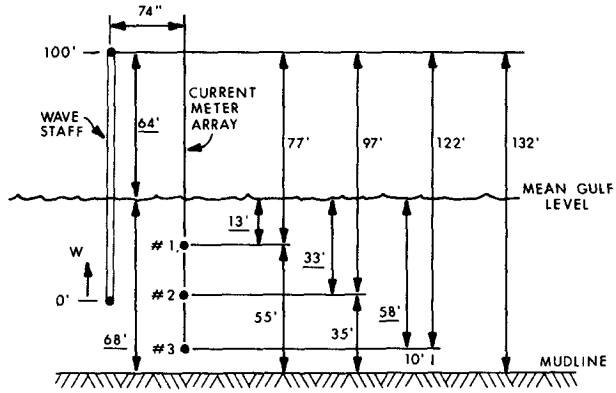

FIG. 5. Current meter depths.

The records from the current meters include motions of two time scales: oscillatory motion associated with the waves and much more slowly varying currents. To separate these effects, some sort of averaging is required; to avoid the side lobes which simple averaging creates, a 249-point numerical filter with a 2 min cutoff was used. The characteristics of the digital filter are shown in Fig. 7. The filter is not very sharp and it might be intuitively thought that the cutoff frequency is too high to properly filter out wave velocities. In fact, over a wide range, the choice of digital filter has very little effect on the resulting currents. Aside from being convenient, this fact confirms the assumption that the separation of the water velocity into wave effects with time scales of a few seconds and currents with time scales of a few hours is a rational method of analysis.

The final calibrated, corrected and filtered currents are shown in Fig. 8. Since the meters measure vector components of velocity, there are two traces for each meter. A positive x signal denotes a north setting current and a positive y signal an east setting current. The scale for the ordinates is in meters per second and the bottom trace is time, with a pulse mark each hour.

West-southwesterly currents over 2 m s^{-1} were observed on the afternoon of 4 September. The strong current persists to near the bottom; 3 m from the bottom, the peak currents are 75% of the near-surface currents. During part of the afternoon the currents were sufficiently large that the total particle velocities, including the oscillatory wave motion, never reversed direction. That is to say, the steady currents were stronger than the orbital velocities of the highest waves.

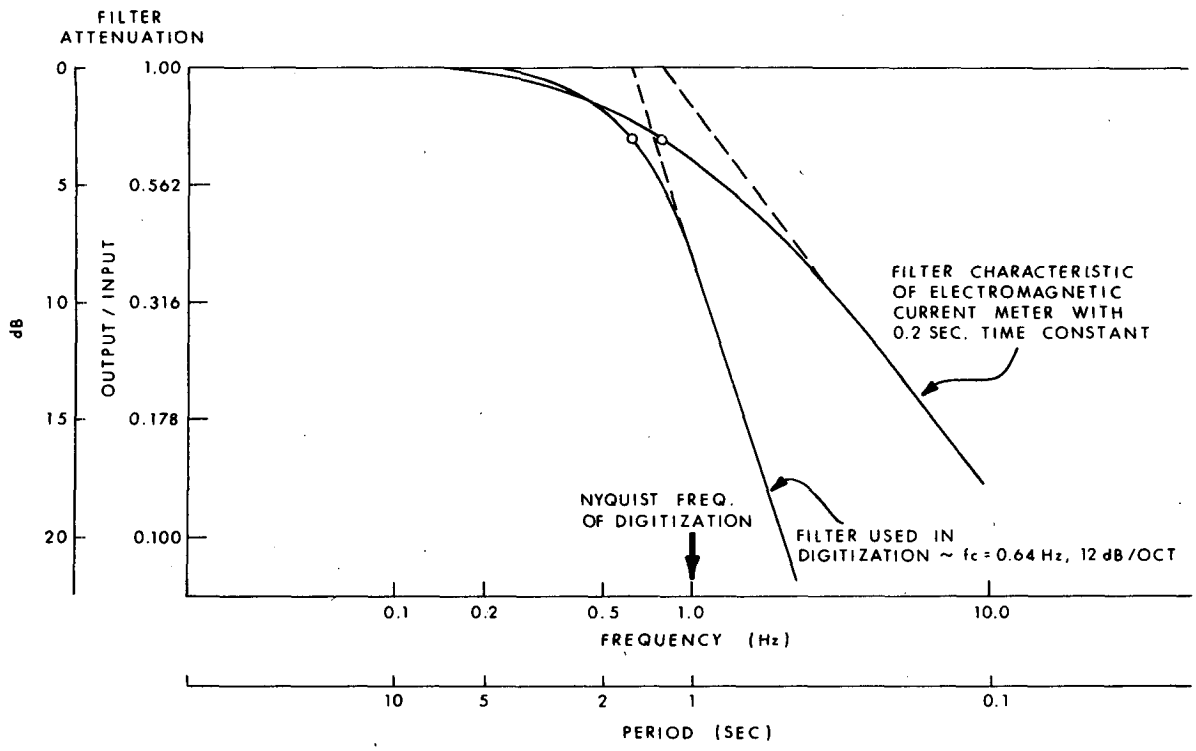

FIG. 6. Characteristics of filters applied to data prior to digitization.

There are other useful ways of presenting the current data. One is the hodograph representation in Fig. 9 where the vector velocities at each meter are shown. The current 13 ft (4 m) deep is given by a small "1," that 33 ft (10 m) deep by a small "2," and that 58 ft (19 m) deep by a small "3." The total water depth is ~68 ft (21 m). Twenty minutes of observed data are given, the samples for each minute being connected by a solid line. This presentation forcefully demonstrates the constancy of the current magnitude through the water column.

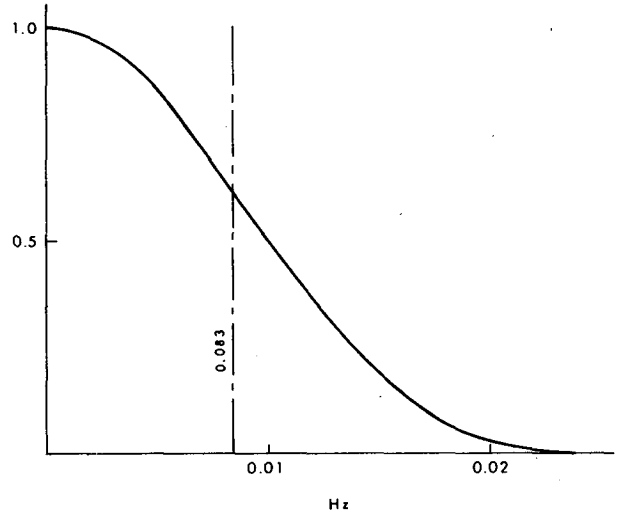

FIG. 7. Attenuation of low-pass filter used to separate currents from wave particle velocities.

5. Preliminary model

The development of a current system in a well-mixed body of water can be described through the use of simplified momentum and continuity equations for fluid flow in a rotating coordinate system:

$$\left.\begin{aligned}\frac{\partial w}{\partial t} &= -ifw+q+\frac{\nu}{H^2}\frac{\partial^2 w}{\partial z^2}\\ \frac{\partial h}{\partial t} &= -H\frac{\partial}{\partial x}\int_{-1}^{0} u\,dz - H\frac{\partial}{\partial y}\int_{-1}^{0} v\,dz\end{aligned}\right\}, \tag{2}$$

where

- w complex horizontal current velocity $[=u+iv]$
- f Coriolis parameter
- q slope of the sea surface
- ν eddy viscosity
- H depth of the basin which was used to non-dimensionalize the vertical coordinate
- z vertical coordinate (zero at the surface)
- h vertical displacement of the water surface.

Two boundary conditions must be specified to solve the momentum equation. At the water surface, the shear stress can be calculated from the local winds. The bottom boundary condition used in the preliminary model was simply that the flow vanished at the bottom.

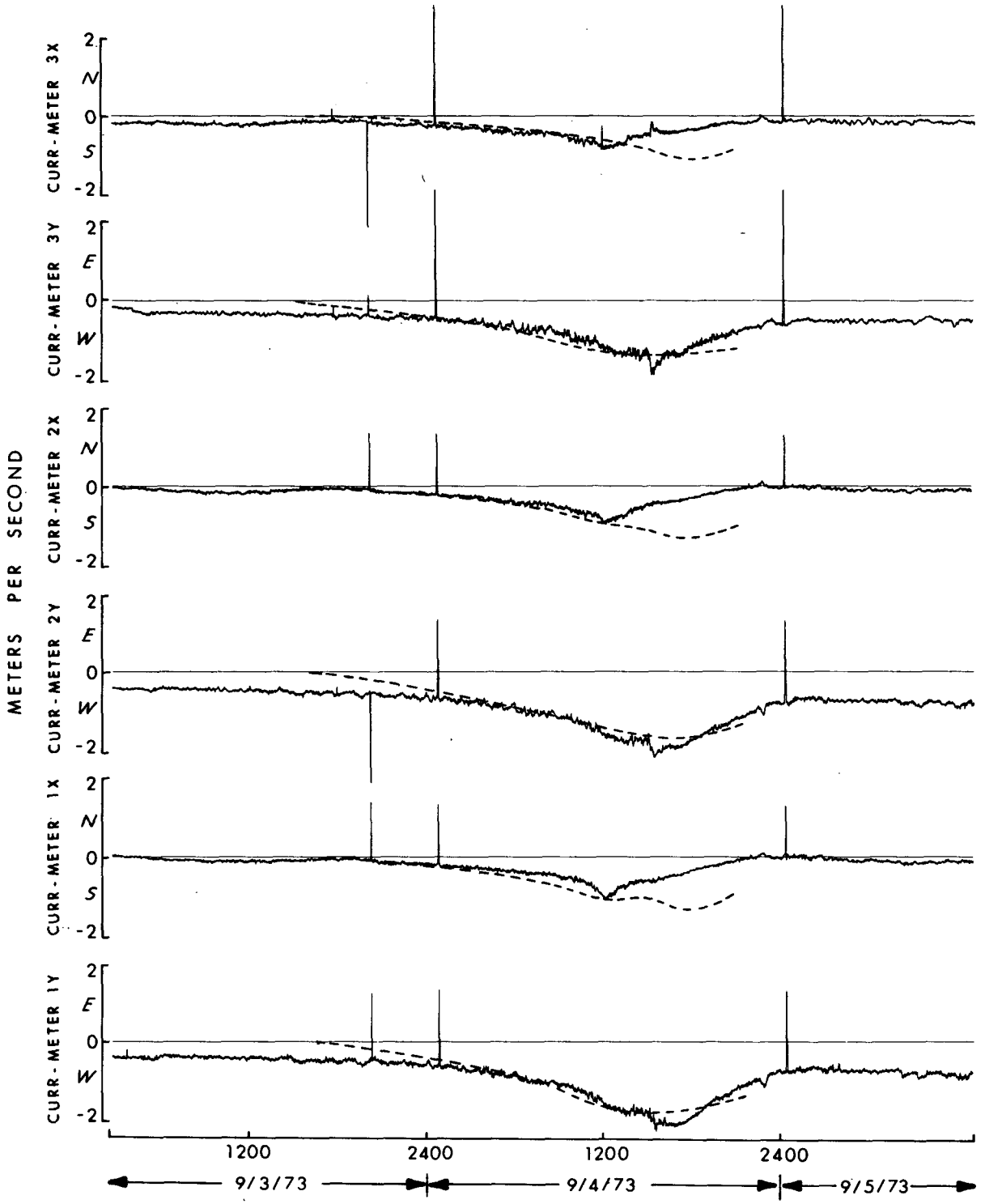

FIG. 8. Measured (solid lines) and final hindcast (dashed lines) currents at Buccaneer during Tropical Storm Delia.

The momentum equation cannot be simply solved for the flow at a point, since the slope q of the surface is related to the currents through the continuity equation. However, the momentum equation can be integrated in the vertical coordinate to permit solution on a two-dimensional finite-difference grid and the vertical current structure then recovered by convolution integrals taken over the calculated history

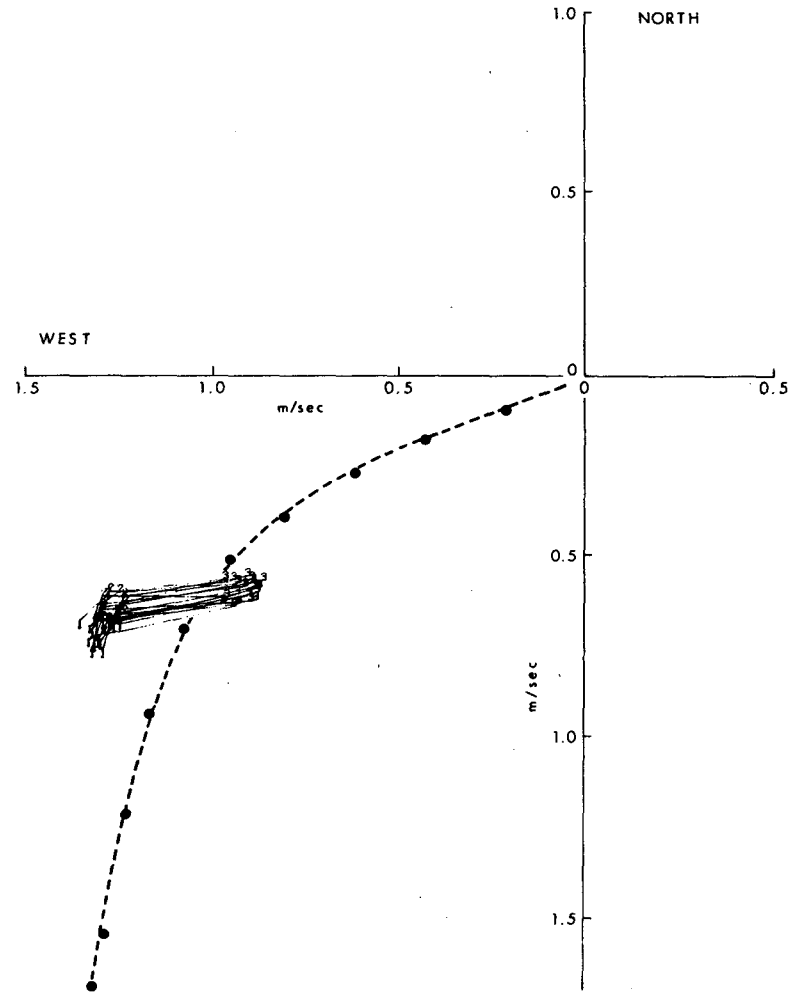

FIG. 9. Measured (solid line) and preliminary hindcast (dashed line) current profiles at Buccaneer, 1200 CDT 9 April 1973.

of surface slope and the wind stress. The assumptions and methods used in the solution have been described in greater detail by Forristall (1974).

A preliminary test of the model was made using a Wilson wind field (Patterson, 1972) based on a storm track taken from National Weather Service advisories. Several problems soon became apparent. The model results are shown as the dashed line in Fig. 9, where the line connects the tips of the calculated current vectors, represented by dots. The cross farthest from the origin gives the surface current and the others show the currents at successive 2 m deeper levels.

Clearly, the observed currents are much more constant with depth than the calculated currents and the direction of the near-surface calculated currents is badly in error. Since the surface currents are strongly influenced by the local winds, it was natural to be suspicious of the wind field used. We thus made an unbiased redetermination of the storm track directly from the available reconnaissance data and the wind measurements at the Buccaneer platform. The aircraft eye fixes support the erratic track shown in Fig. 3, with alternating periods of slow looping motion and rather fast relatively straight motion. These track characteristics were corroborated by the wind trace at Buccaneer, which showed responses to the departure of the storm track from a simple approach to the station.

The wind field was recomputed using the method of Cardone *et al.* (1976) which is an application of the theoretical model of horizontal air flow in the boundary layer of a moving vortex, as derived originally by Chow (1971). The model requires as input a specification of storm track and pressure field. The latter is prescribed by the pressure drop across the storm, the scale of the pressure field (which is defined by the scale radius of an exponential radial pressure profile), and the magnitude and orientation of the

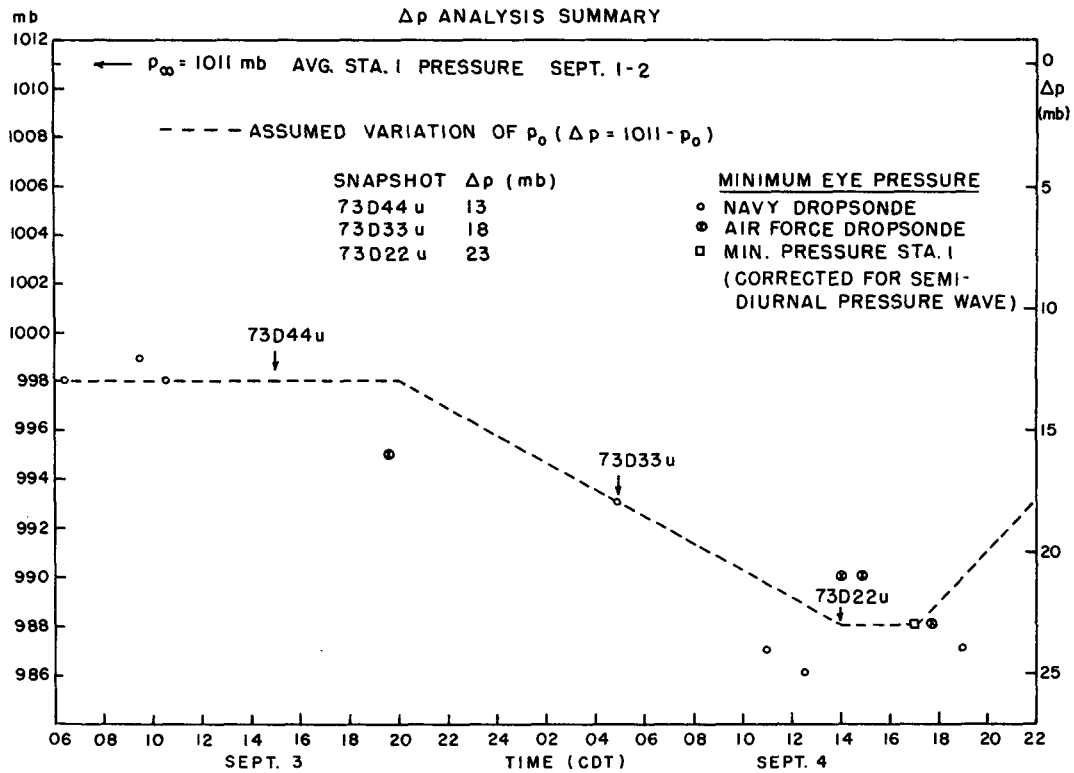

FIG. 10. Central pressure in Tropical Storm Delia.

large-scale ambient pressure field or geostrophic "steering" current in which the storm is embedded.

The available central pressure data suggest that Delia intensified in the 24 h period prior to landfall, as shown in Fig. 10. After consideration of the error typical of dropsonde determinations of minimum sea level pressure, the minimum pressure observed at Buccaneer is consistent with the aircraft data, and

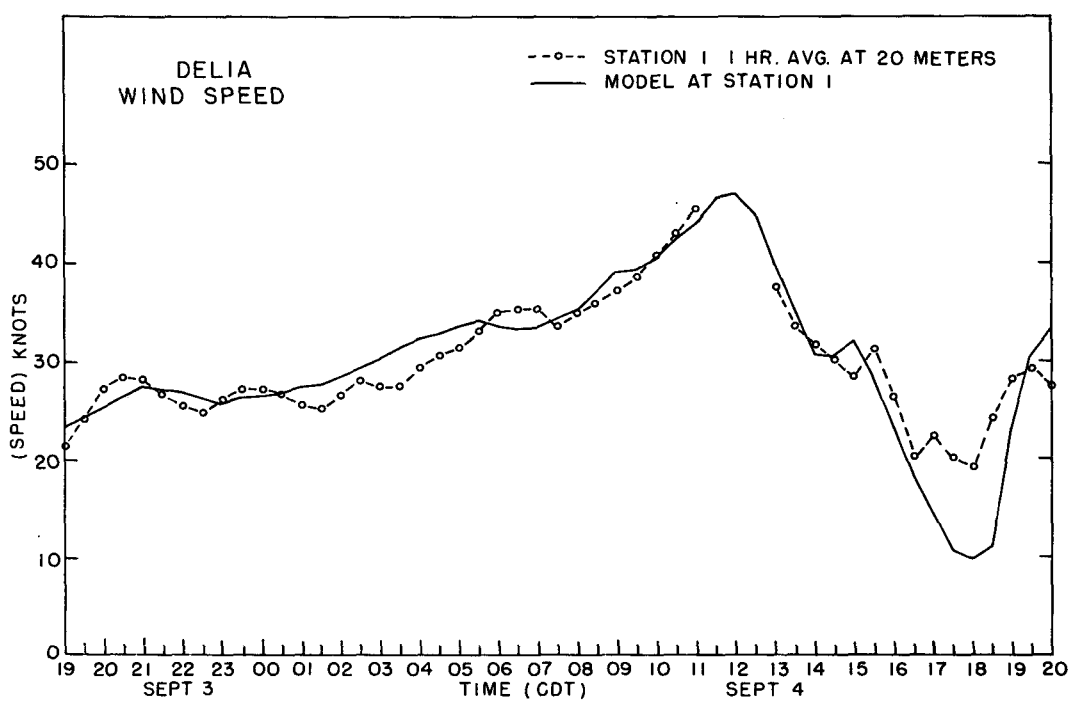

FIG. 11. Delia wind speed.

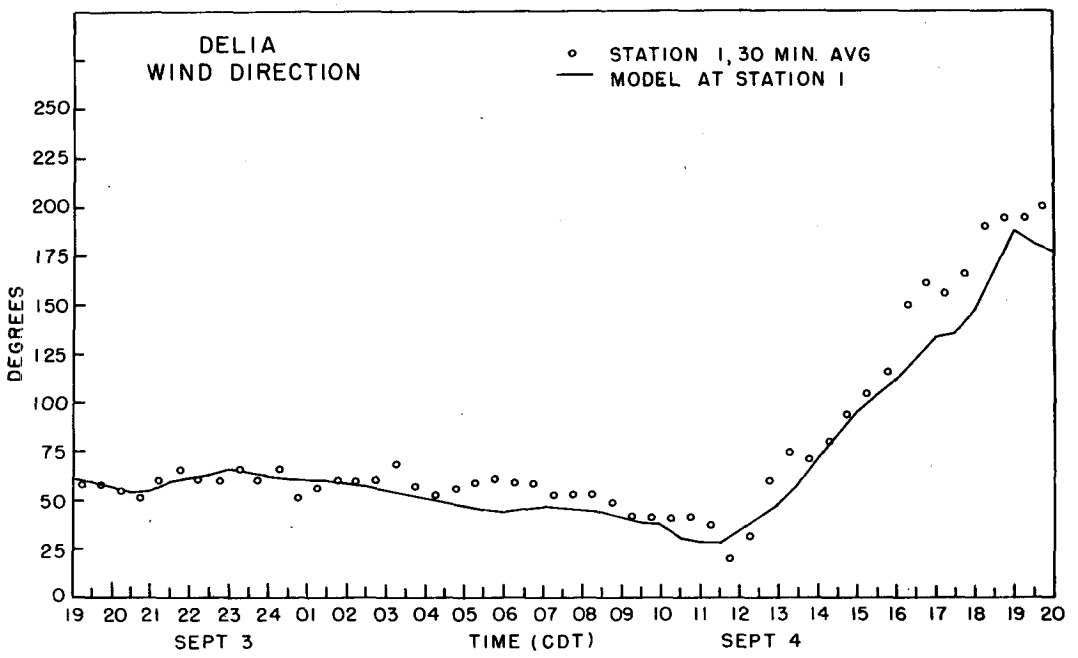

FIG. 12. Delia wind direction.

because of Delia's large eye is probably within a few tenths of a millibar of the true minimum central pressure.

The specification of the scale radius of the pressure profile was based mainly on the timing of occurrence of maximum sustained winds at Buccaneer and Galveston, with respect to the storm track. At the Galveston airport weather station these occurred near 1400 CDT, while at Buccaneer maximum winds probably occurred near 1200 CDT, although the upwind tower obstruction near then makes that timing uncertain. Nevetheless, both observations support a large radius of maximum winds (~40 mi). The corresponding scale radius for the pressure profile is 55 mi.

Despite the erratic track of Delia, the surface synoptic charts for the eastern United States showed Delia's circulation at low levels to be embedded in a steady steering current throughout the period of interest. This current was chosen to have a geostrophic magnitude of 6 m s^{-1}. This value is consistent with the wind observed at Buccaneer for several days prior to the influence of Delia.

Given these storm parameters, the quasi-steady-state wind model was solved for three characteristic states[1], as shown in Fig. 10, from which were interpolated the time history of anemometer level (20 m) wind speed and direction. After 1800 on 4 September, the interpolation was between states 73D22u and 73D33u. Comparison of measured (adjusted to 20 m level) and modeled wind speed and direction at Buccaneer are shown in Figs. 11 and 12.

The surface boundary layer model developed by Cardone (1969) effectively relates the wind at anemometer height to the surface stress through the use of an implied drag coefficient that is itself a function of wind speed and stability. For the relatively small air-sea temperature differences characteristic of hurricanes and moderate to high winds, the neutral stability relationships can be used with insignificant error. The surface stress calculated in this manner was used as the input to the current model.

Model runs with the new wind field had much better directional accuracy, but no improvement in depth dependence. There is essentially only one free parameter for calibration purposes in Eq. (2), the vertical eddy viscosity ν. Increasing the viscosity will bring the velocities at various depths closer together, but never match the observations in Fig. 9.

It might be thought that the imposition of a constant eddy viscosity was the cause of the errors. However, subsequent measurements have shown that the water at Buccaneer is usually well mixed all the way to the bottom even in calm weather. Although no salinity or temperature measurements were made during the storm, it is quite reasonable to suppose that the high wind and waves resulted in a high eddy viscosity which remained constant to near the bottom. This hypothesis is, in fact, supported by the near constancy of the measured currents with depth.

The strong near-bottom flow suggests that the dynamics of the bottom boundary layer are important

[1] The states are called "snapshots" in Fig. 10 and are labeled by codes beginning with 73D to denote the "D" storm of 1973.

in the solution and that the formulation in the preliminary model may be too simplistic. That model simply assumed no flow at the physical bottom, which should be true in a literal sense. However, the dynamics near the bottom may be such that no slip and a constant eddy viscosity are a poor parameterization of the actual situation.

6. Bottom boundary layer dynamics

The turbulent boundary layer in the atmosphere has received much study (Monin, 1970) and the basic formulation has recently been extended to the benthic boundary layer of the Florida current by Weatherly (1972). Here we briefly review this theory and check its applicability to measurements during Delia.

In a turbulent boundary layer, the shear stress is a constant τ_0 from which the friction velocity u_* can be defined as

$$u_* = (\tau_0/\rho)^{\frac{1}{2}}. \tag{3}$$

The speed distribution in the layer is then given by

$$u(z) = (u_*/\kappa) \log(z/z_0), \tag{4}$$

where $\kappa = 0.4$ is von Kármán's constant, z_0 the roughness height and z the measured distance upward from the bottom. For hydrodynamically rough flow, experiments indicate that

$$z_0 \approx d/30, \tag{5}$$

where d is the scale of the bottom roughness elements. In geophysical flows dominated by the Coriolis effect, the boundary layer thickness δ does not increase downstream (Csanady, 1967), but is limited to about

$$\delta \approx u_*^2/fU, \tag{6}$$

where U is the geostrophic velocity away from the boundary layer.

If we make the assumption, which Fig. 13 shows to be consistent with the data, that u_* is on the order of 0.05 m s^{-1} for $U = 2$ m s^{-1}, then Eq. (6) yields $\delta = 20$ m, which is roughly the water depth at Buccaneer. Obviously, the boundary layer cannot be expected to extend all the way to the free surface, where direct wind shear dominates, but the theory indicates that the records from the two lowest meters should at least be dominated by boundary layer effects. To study these assumptions, we took 1 h averages of the currents and fit (4) to either the two lowest meters or all three meters. The resulting time histories of u_* and z_0 are given in Figs. 13 and 14. The values of u_* are in the range assumed and increase as expected during the storm. However, the calculated values of z_0

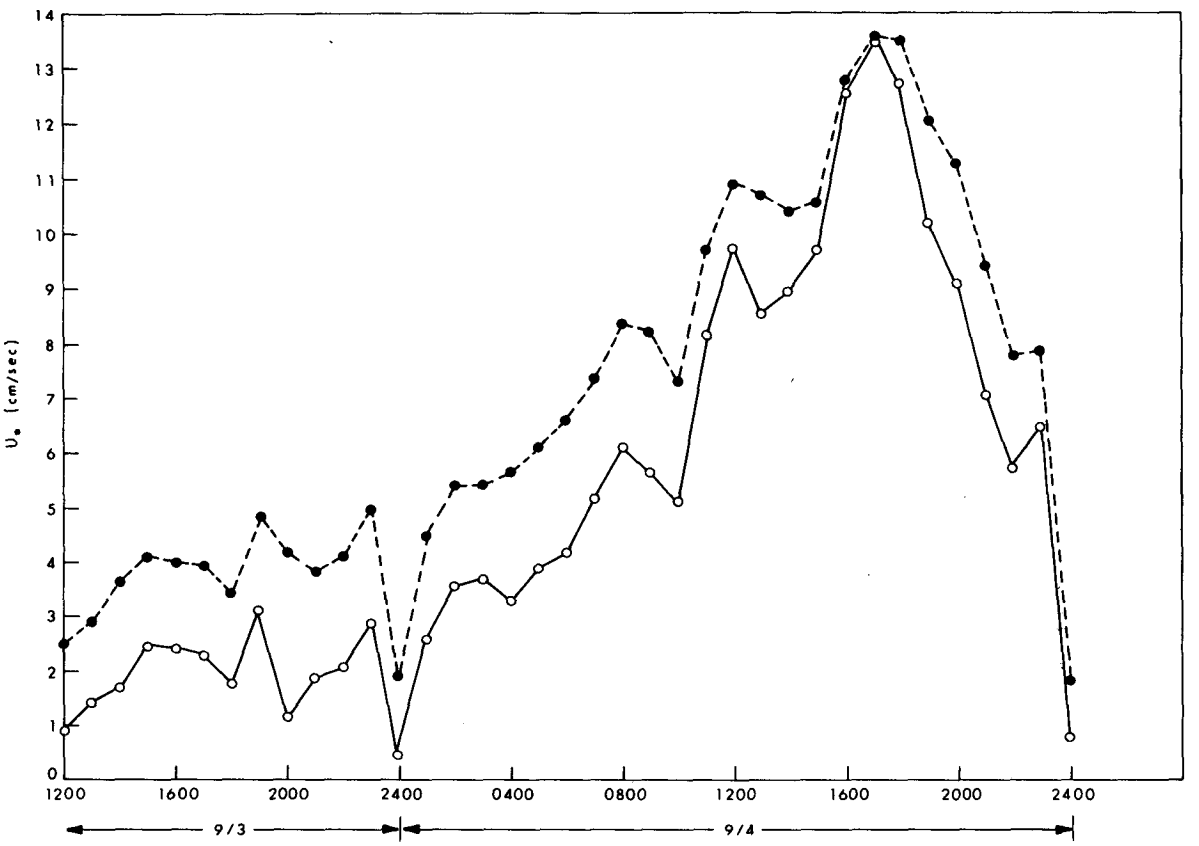

FIG. 13. Friction velocity calculated from all three meters (solid line) and from lowest two meters (dashed line).

behave rather strangely. Not only does z_0 fluctuate wildly instead of remaining constant, but also it is generally predicted to be much too large. For $z_0=5$ cm, Eq. (5) indicates that the bottom roughness elements must be on the order of 1.5 m, which is clearly unreasonable for a smooth clay bottom.

It is not too difficult to find a reason for the observations not being consistent with the theory, since the theory was developed for stationary conditions. Weatherly (1972) expressed concern that tidal fluctuations might weaken the applicability of the theory and the situation is much worse in the present instance. Study of the unfiltered velocity data from the bottom current meter reveals that velocity oscillations due to the large surface waves extend at least that deep and are of the same order of magnitude as the currents. In laboratory situations where the Coriolis effect is not important, turbulent boundary layers are observed to thicken downstream according to the formula

$$\delta \approx \frac{u_*}{U} x, \tag{7}$$

where x is the distance downstream.

The thickness in Eq. (6) is a limiting value for this growth due to the dominance of the Coriolis effect in geophysical flows. If the flow is rapidly oscillating, the boundary layer may not have time to grow to the limit. For a sinusoidally oscillating flow with peak velocity of 1 m s^{-1} and period of 10 s, the maximum distance downstream before flow reversal is about 3 m. Thus it is appropriate to use (7) to estimate the boundary layer thickness during storms in relatively shallow water. Using $u_*/U=0.03$ as before, Eq. (7) gives $\delta \approx 10$ cm, so that the boundary layer actually lies far below the bottom current meter.

We are thus faced with a rather serious difficulty. The preliminary model work showed that the bottom boundary layer must be taken into account, but it seems that we do not have data from that layer. It is, however, possible to make some heuristic arguments and conjectures which lead to a testable hypothesis for the influence of the boundary layer on the body of the flow.

To close the solution for the flow profile, we require a bottom boundary condition which relates the shear stress at the bottom to a calculated velocity. From Eqs. (3) and (4) we have

$$\tau_0=\rho u_*^2=\rho\kappa u(\delta)[u_*/\log(\delta/z_0)], \tag{8}$$

where δ, as before, is the distance to the top of the boundary layer. Now, as the mean flow velocity increases with storm intensity, both wave height and period will also increase, and [from (7)] δ will in-

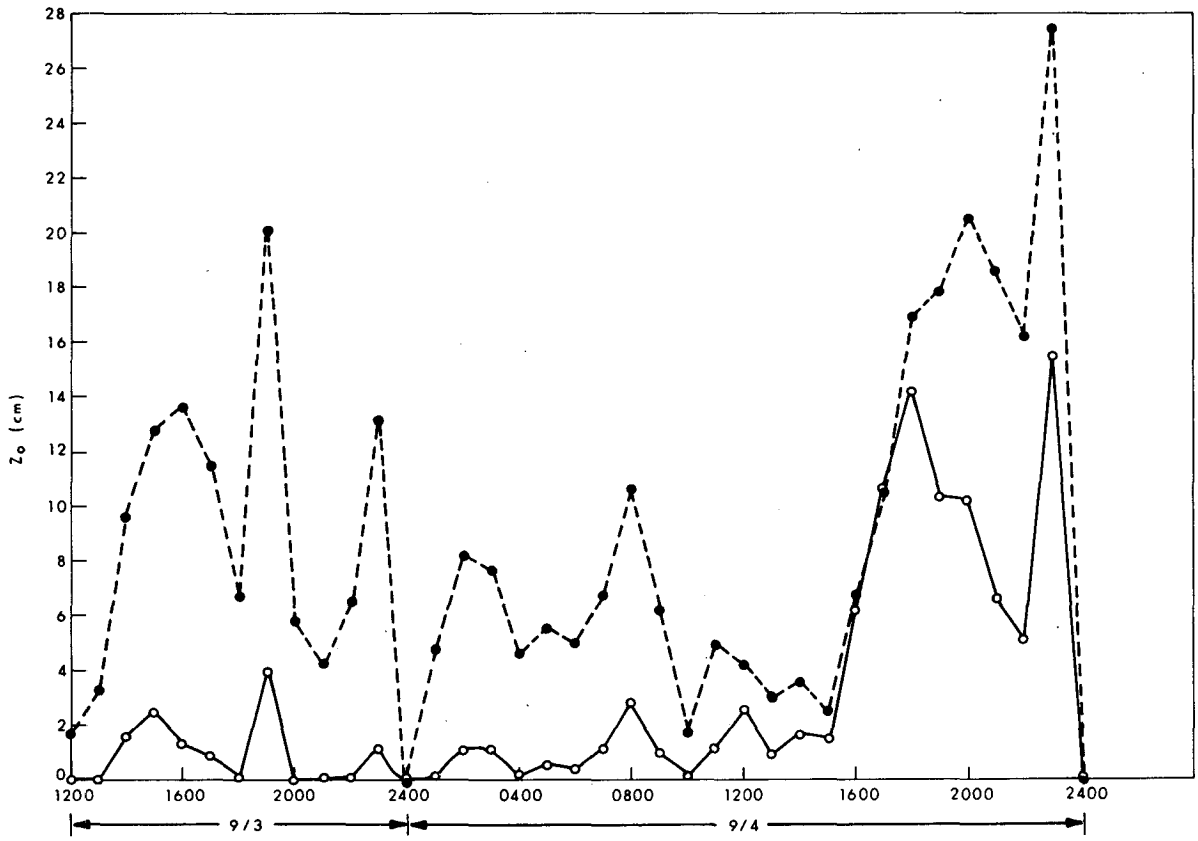

FIG. 14. As in Fig. 13 except for roughness height.

crease. It is thus at least possible to conjecture that the bracketed term in Eq. (8) will remain roughly constant throughout the storm. It does not seem possible to test the accuracy of the conjecture directly. Its worth is best tested by judging the accuracy of a model which includes it. The construction of such a model is reasonably simple since the conjecture results in proportionality between bottom shear and bottom velocity. Since δ is very small relative to the total depth, we can further simplify matters by assuming that the boundary condition is always applied exactly at the bottom rather than at the top of the thin boundary layer. Thus

$$\tau(0)/\rho=\epsilon u(0), \tag{9}$$

where ϵ is a constant with dimensions of velocity whose magnitude will be determined by fitting the model to the observed currents. A formulation similar to (9) has been used by others including Jelesnianski (1967), but there seems to be no physical justification of it in print.

It is now necessary to incorporate boundary condition (9) into the computer model. Analytical solutions for pure drift and slope currents must be calculated and the bottom drag term in the finite difference model must be reformulated.

a. Drift currents

For a pure wind drift current, Eq. (2) reduces to

$$\frac{\partial w}{\partial t}=-ifw+\frac{\nu}{H^2}\frac{\partial^2 w}{\partial z^2}, \tag{10}$$

where the vertical coordinate has been nondimensionalized with respect to the depth H, so that now $z=0$ at the free surface and $z=-1$ at the bottom.

If the applied surface stress is a constant, the upper boundary condition (iF_0) will be

$$\frac{\nu}{H}\frac{\partial w}{\partial z}\bigg|_{z=0}=iF_0. \tag{11}$$

In the present notation, the bottom boundary condition (9) becomes

$$\frac{\partial w}{\partial z}\bigg|_{z=-1}=\frac{\epsilon H}{\nu}w\bigg|_{z=-1}. \tag{12}$$

Taking a Laplace transform reduces Eqs. (10)–(12) to

$$\left.\begin{aligned}&\frac{\partial^2\bar{w}}{\partial z^2}=\beta^2\bar{w},\quad \text{where}\quad \beta^2=H^2(s+if)\nu^{-1}\\ &\frac{\partial\bar{w}}{\partial z}\bigg|_{z=0}=\frac{iF_0H}{s\nu}\equiv\frac{A}{s}\\ &\frac{\partial\bar{w}}{\partial z}\bigg|_{z=-1}=\frac{\epsilon H}{\nu}\bar{w}\bigg|_{z=-1}\equiv\alpha\bar{w}|_{z=-1}.\end{aligned}\right\} \tag{13}$$

These transformed equations are easily solved to yield

$$\bar{w}=\frac{A}{\beta s}\left[\frac{\alpha\sinh\beta(1+z)+\beta\cosh\beta(1+z)}{\alpha\cosh\beta+\beta\sinh\beta}\right]. \tag{14}$$

To invert (14) by the inversion integral, we need the location of the zeros of $\alpha\cosh\beta+\beta\sinh\beta$, which amounts to solving

$$\beta\tanh\beta=-\alpha \tag{15}$$

for β, with α positive and real. Now, if $\beta=x+iy$, Eq. (15) becomes

$$\frac{\sinh 2x+i\sin 2y}{\cosh 2x+\cos 2y}=-\alpha\frac{x-iy}{x^2+y^2}.$$

Note that both denominators are always real and positive. Then, considering real parts, the sign of $\sinh(2x)$ must equal the sign of $(-\alpha x)$. This is possible only for $x=0$. Thus, any β which solves (15) must be purely imaginary, and if $\beta=iy$, Eq. (15) reduces to

$$y\tan y=\alpha. \tag{16}$$

The solutions to this transcendental equation are easily found numerically, with one solution y_n in each interval

$$[n\pi,\ (n+\tfrac{1}{2})\pi].$$

Then, using the inversion integral and the residue theorem, the inverse transform of (14) is

$$w=\frac{A}{\gamma}\left[\frac{\alpha\sinh\gamma(1+z)+\gamma\cosh\gamma(1+z)}{\alpha\cosh\gamma+\gamma\sinh\gamma}\right]+\frac{2iF_0}{H}\times\sum_{n=1}^{\infty}\frac{\alpha\sin y_n(1+z)+y_n\cos y_n(1+z)}{(\alpha+1)\sin y_n+y_n\cos y_n}\frac{e^{s_nt}}{s_n}, \tag{17}$$

where $\gamma=H(if/\nu)^{\frac{1}{2}}$. If the forcing function is not constant, i.e., if

$$\frac{\partial\hat{w}}{\partial z}\bigg|_{z=0}=\frac{H}{\nu}F(t),$$

then the solution is

$$\hat{w}=\frac{1}{iF_0}\int_0^t F(t-\tau)\frac{\partial}{\partial\tau}w(\tau)d\tau. \tag{18}$$

Examples of the analytic solution in Eq. (17) are shown in Fig. 15, 12 h after a steady 20 m s^{-1} wind begins blowing over a 20 m deep ocean. The presentation is similar to that in Fig. 9. The calculated currents are vastly different for different slip coefficients, with $\epsilon=0.005$ representing very limited slip and $\epsilon=10^{-5}$ giving almost pure slip. For the latter case, the flow is almost entirely isolated from the damping influence of bottom friction, and oscillations dependent on the Coriolis parameter dominate the

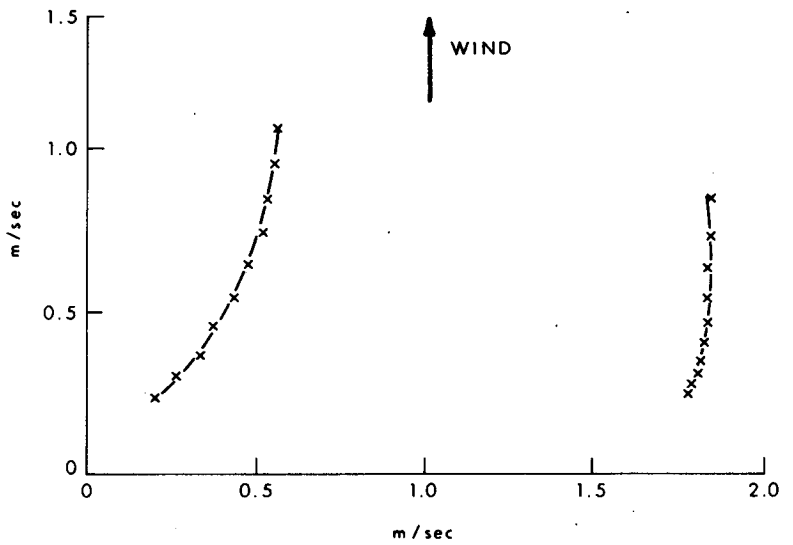

FIG. 15. Effect of slip condition of drift current hodographs: $\epsilon=0.005$ (left) and $\epsilon=10^{-5}$ (right).

development of the flow. These effects are most important in relatively shallow water, such as at Buccaneer.

b. Slope currents

If the sea surface is not level, its slope q will appear as a body force in Eq. (2). Taking $q=q_0$ constant for the moment, with zero wind stress and the bottom boundary condition of (12), the solution in the Laplace transform plane is

$$\bar{w}=q_0[s(s+if)]^{-1}\left(\frac{\beta\sinh\beta+\alpha\cosh\beta-\alpha\cosh\beta z}{\beta\sinh\beta+\alpha\cosh\beta}\right). \quad (19)$$

The series of poles is the same as in (14) and the inverse is found similarly to be

$$w=\frac{q_0}{if}\left(\frac{\gamma\sinh\gamma+\alpha\cosh\gamma-\alpha\cosh\gamma z}{\gamma\sinh\gamma+\alpha\cosh\gamma}\right)$$
$$+2q_0\sum_{n=1}^{\infty}\frac{e^{\epsilon n t}}{s_n y_n}\left[\frac{y_n\sin y_n-\alpha\cos y_n+\alpha\cos y_n z}{(\alpha+1)\sin y_n+y_n\cos y_n}\right]. \quad (20)$$

When the surface slope is not constant, a convolution integral over (20) is used in (18). Variation of the slip coefficient again has a large effect on the solutions.

7. Depth-integrated solution

The sum of the drift current calculated from Eq. (17) and the slope current calculated from Eq. (20) should give the history of the wind-driven currents at any depths at the Buccaneer site. However, in order to use (20), it is necessary to know the history of the surface slope at the site. Since the storm surge and thus surface slope are related to the integrated currents through the continuity equation, the storm surge equations must be solved for an area surrounding the site before (20) is applied.

Integrating Eq. (2) vertically from bottom to surface gives

$$\frac{\partial W}{\partial t}=-ifW+Q+F-C, \quad (21)$$

where the transport is

$$W=H\int_{-1}^{0}w dz,$$

$Q=Hq$, F is the wind shear stress, and the bottom stress is

$$C=\frac{\nu}{H}\frac{\partial w}{\partial z}\bigg|_{z=-1}. \quad (22)$$

Eq. (21) and the continuity equation can be solved by a two-dimensional finite-difference scheme for $q(t)$. The most interesting part of the solution is the calculation of the boundary stress. There are various ways of estimating the drag from the transport, but for consistency with the analytically calculated currents, the drag must be found from (12). This can be done by extending the bottom friction calculation due to Jelesnianski (1970) to the case of a slip boundary condition. From Eq. (12)

$$C=\epsilon w|_{z=-1}. \quad (23)$$

The drag may be broken down into parts associated with the slope and drift components of the current. From (17) and (18), the drift current component of the drag is

$$C_d=\frac{2\epsilon}{H}\int_0^t F(t-\tau)K_F(\tau)e^{-if\tau}d\tau, \quad (24)$$

where

$$K_F(\tau)=\sum_{n=1}^{\infty} y_n[(\alpha+1)\sin y_n+y_n\cos y_n]^{-1} \times\exp(-y_n^2\nu\tau/H^2).$$

For the slope current drag, (20) similarly yields

$$C_s=2\epsilon\int_0^t q(t-\tau)K_Q(\tau)e^{-if\tau}d\tau, \quad (25)$$

where

$$K_Q(\tau)=\sum_{n=1}^{\infty}\frac{\sin y_n}{(\alpha+1)\sin y_n+y_n\cos y_n}\exp(-y_n^2\nu\tau/H^2).$$

Integration of (24) and (25) at each time step and grid point would be extremely wasteful of computer time and storage if a significant number of terms from the series were required. Fortunately, Jelesnianski (1970) developed a reasonably simple method of approximation which was also used by Forristall (1974). The character of the kernels and their infinite integral over τ are preserved by taking

$$K_F\approx B[\exp(-y_1^2\nu\tau/H^2)-\exp(-b\nu\tau/H^2)], \quad (26)$$

where

$$B=y_1[(\alpha+1)\sin y_1+y_1\cos y_1]^{-1},$$

$$b=-B\left\{\sum_{n=2}^{\infty}\frac{1}{y_n}[(\alpha+1)\sin y_n+y_n\cos y_n]^{-1}\right\}^{-1},$$

$$K_Q(\tau)\approx y_1^2\left[\sum_{n=1}^{\infty}\frac{1}{y_n^2}\frac{\sin y_n}{(\alpha+1)\sin y_n+y_n\cos y_n}\right] \times\exp(-y_1^2\nu\tau/H^2). \quad (27)$$

The recursion scheme for exponential kernels developed by Jelesnianski is then used to calculate C as the solution progresses.

The finite-difference equations were solved on a square grid with a grid size of 11.59 km, which extended from 25°45′ to 30°0′N, and from 90°0′ to 97°23′W. The explicit integration of the storm surge necessitated a short time step of 150 s. Land boundaries and bathymetry were hand digitized to the grid. Transports normal to the boundaries were set equal to zero. The eastern and southern boundaries of the grid are in open water, where it is difficult to specify a correct lateral boundary condition. We set the derivative of velocity normal to these boundaries equal to zero. Although this boundary condition causes the reflection of long waves (Reid, 1975), it permits forced flow through the boundaries. In any case the boundaries were far enough from Buccaneer that the reflections did not seriously corrupt the solution there for the 30 h integration time.

It should be noted that the finite-difference solution gives the transport as well as the surface slope. After the drift and slope currents are calculated, they may be vertically integrated to again obtain the transport. Since the two approaches are consistent, the two derivations should agree, and in fact they do to within a few percent. The small discrepancy that does exist is due primarily to the weak smoothing used in the finite difference scheme.

8. Effect on Delia hindcasts

With these new features incorporated in the basic current model, several additional computer hindcasts were made. The magnitudes of the eddy viscosity ν and the slip coefficient ϵ are poorly known from theory, so they can be used in a sense as tuning parameters for the model. Indeed, study of current data during strong winds is probably the best method of investigating these important physical parameters. In broad terms, increasing the eddy viscosity causes the currents to be more uniform with depth and decreasing the slip coefficient increases the near bottom currents. The combination of these factors which gave the best fit to the Delia data was $\nu=0.03$ m^2 s^{-1} and $\epsilon=0.001$ m s^{-1}. Note that this value of the eddy viscosity is over four orders of magnitude larger than the molecular viscosity of water. It is also considerably larger than the eddy viscosity which might be estimated from the Reynolds number of the flow. The observed eddy viscosity might possibly be explained by the additional turbulence introduced by the surface waves.

The results of a hindcast using these values are shown in Fig. 8, which compares the current meter output to vector components calculated for the depths at which the meters were located. The agreement between the two is very good for the buildup of the storm and the proper depth dependence has been achieved. However, the southward component of the flow continues to increase after the peak of the storm and is much too large at the end of the hindcast.

The flow during the peak of the storm is essentially longshore and parallel to the bathymetric contours. The direct response to the local wind is augmented by the geostrophic balance between the storm surge and the longshore current. These features are correctly modeled, but after the peak of the storm the hindcast currents shift to be more southward and fail to decay as rapidly as the observations. Assuming that the anchor rotation occurred at the end of the storm does not improve the comparisons. The finite difference scheme used in the model might be the source of some of this discrepancy, since it uses simple forward time steps with centered space differences on an unstaggered grid. More sophisticated schemes have been developed by many workers, including Heaps (1969) and Leendertse (1967). In an effort to improve

the accuracy of the computations, some numerical features from other models were tested.

In particular, a staggered grid system, centered time differencing and the open water boundary condition suggested by Reid (1975) were tested, both alone and in combination. While these numerical changes did affect the solution somewhat, none produced a markedly better match with the data. It seems likely that the problem is due not to numerical difficulties, but rather to some dissipation process which has not yet been properly modeled. Fortunately, the buildup to peak conditions, which is of the greatest practical interest, has been hindcast quite accurately using simple parameterizations of the physical processes.

Acknowledgments. A truthful Acknowledgments Section for a project of this magnitude would rival the paper in length. However, the contributions of a few individuals were so great that they must be recognized. J. M. Hall was largely responsible for the design and installation of the measurement stations. T. E. Long worked untiringly to make the instrumentation work as it was designed to. C. A. Gutierrez did much of the data analysis and filled in ably offshore when necessary. The helpfulness and cooperation of the operating personnel in the Southern Region of Shell Oil Company were vital to the project. W. B. Ingram, R. P. Nordgren and E. G. Ward made helpful comments on an earlier version of the manuscript. The program has been monetarily supported by Shell Oil Company, Exxon Production Research Company, Chevron Oil Field Research Company, Mobil Research and Development Company, Amoco Production Company and Seadock Inc.

REFERENCES

Cardone, V. J., 1969: Specification of the wind distribution in the marine boundary layer for wave forecasting. TP-69-1, Geophysical Sciences Laboratory, New York University, 137 pp. [NTIS No. AD702490].

——, W. J. Pierson and E. G. Ward, 1976: Hindcasting the directional spectra of hurricane-generated waves. *J. Pet. Tech.*, **28**, 385–394.

Chow, S., 1971: A study of the windfield in the planetary boundary layer of a moving tropical cyclone. MS thesis, Dept. of Meteorology and Oceanography, New York University, 58 pp.

Csanady, G. T., 1967: On the "resistance law" of a turbulent Ekman layer. *J. Atmos. Sci.*, **24**, 467–471.

Forristall, G. Z., 1974: Three-dimensional structure of storm generated currents. *J. Geophys. Res.*, **79**, 2721–2729.

Hall, J. M., 1972: Hurricane generated ocean currents. *Proc. Fourth Annual Offshore Tech. Conf.*, Paper 1518, Dallas, Tex., 69–77.

Heaps, N. S., 1969: A two-dimensional numerical sea model. *Phil. Trans. Roy. Soc. London*, **A265**, 93–137.

Jelesnianski, C. P., 1967: Numerical computations of storm surges with bottom stress. *Mon. Wea. Rev.*, **95**, 740–756.

——, 1970: Bottom stress time history in linearized equations of motion for storm surges. *Mon. Wea. Rev.*, **98**, 462–478.

Leendertse, J. J., 1967: Aspects of a computational model for long period water-wave propagation. Memo. RM 5294-PR, The Rand Corporation, Santa Monica, Calif., 165 pp.

Monin, A. S., 1970: The atmospheric boundary layer. *Annual Reviews of Fluid Mechanics*, Vol. 2, Annual Reviews, 225–250.

Patterson, M. M., 1972: Hurricane hindcasting in the Gulf of Mexico. *Soc. Pet. Engr. J.*, **12**, 321–328.

Reid, R. O., 1975: Comments on "Three-dimensional structure of storm-generated currents" by G. Z. Forristall. *J. Geophys. Res.*, **8**, 1184–1185.

Weatherly, G. L., 1972: A study of the bottom boundary layer of the Florida current. *J. Phys. Oceanogr.*, **2**, 54–72.